An N-terminal Ca^{2+}-binding motif regulates the secretory pathway Ca^{2+}/Mn^{2+}-transport ATPase SPCA1

Received for publication, October 12, 2018, and in revised form, March 23, 2019 Published, Papers in Press, March 28, 2019, DOI 10.1074/jbc.RA118.006250

Jialin Chen[‡], Susanne Smaardijk[‡], Charles-Alexandre Mattelaer[§1], Filip Pamula[‡], Ilse Vandecaetsbeek[‡], Jo Vanoevelen[‡], Frank Wuytack[‡], Eveline Lescrinier[§], Jan Eggermont[‡], and Peter Vangheluwe[‡2]

From the [‡]Laboratory of Cellular Transport Systems, Department of Cellular and Molecular Medicine and [§]Medicinal Chemistry, Department of Pharmaceutical and Pharmacological Sciences, Rega Institute, KU Leuven, Belgium

Edited by Phyllis I. Hanson

The Ca^{2+}/Mn^{2+} transport ATPases 1a and 2 (SPCA1a/2) are closely related to the sarco(endo)plasmic reticulum Ca^{2+}-ATPase (SERCA) and are implicated in breast cancer and Hailey–Hailey skin disease. Here, we purified the human SPCA1a/2 isoforms from a yeast recombinant expression system and compared their biochemical properties after reconstitution. We observed that the purified SPCA1a displays a lower Ca^{2+} affinity and slightly lower Mn^{2+} affinity than SPCA2. Remarkably, the turnover rates of SPCA1a in the presence of Mn^{2+} and SPCA2 incubated with Ca^{2+} and Mn^{2+} were comparable, whereas the turnover rate of SPCA1a in Ca^{2+} was 2-fold higher. Moreover, we noted an unusual biphasic activation curve for the SPCA1a ATPase and autophosphorylation activity, not observed with SPCA2. We also found that the biphasic pattern and low apparent ion affinity of SPCA1a critically depends on ATP concentration. We further show that the specific properties of SPCA1a at least partially depend on an N-terminal EF-hand–like motif, which is present only in the SPCA1a isoform and absent in SPCA2. This motif binds Ca^{2+}, and its mutation lowered the Ca^{2+} turnover rate relative to that of Mn^{2+}, increased substrate affinity, and reduced the level of biphasic activation of SPCA1a. A biochemical analysis indicated that Ca^{2+} binding to the N-terminal EF-hand–like motif promotes the activity of SPCA1a by facilitating autophosphorylation. We propose that this regulation may be physiologically relevant in cells with a high Ca^{2+} load, such as mammary gland cells during lactation, or in cells with a low ATP content, such as keratinocytes.

Transient alterations in subcellular Ca^{2+} concentrations drive numerous physiological processes. The local Ca^{2+} levels in cells are tightly regulated by membrane transport proteins such as ion channels, exchangers, and active transport ATPases (1, 2). Among them, the Ca^{2+} transport ATPases utilize the energy released from ATP hydrolysis to pump Ca^{2+} ions against the concentration gradient, *i.e.* from the cytosol to the exoplasmic compartments. In humans, three types of Ca^{2+}-ATPases were identified that are localized in distinct membrane compartments: the closely related P2A-type ATPases sarco(endo-)plasmic reticulum Ca^{2+}-ATPase (SERCA)[3] and secretory pathway Ca^{2+}-ATPase (SPCA), sharing 29% sequence identity and over 40% sequence similarities, and the P2B-type ATPase plasma membrane Ca^{2+}-ATPase (PMCA), which is more distantly related (3). All Ca^{2+}-ATPases undergo transient autophosphorylation during the transport cycle.

The SPCA pumps are located in later compartments of the Golgi/secretory pathway and transport both Ca^{2+} and Mn^{2+} ions with high affinities, which represents a unique feature among the Ca^{2+} transport ATPases. SPCA isoforms ensure a constant filling of the Golgi and secretory pathway with Ca^{2+} and also Mn^{2+}. Both ions are cofactors of many Golgi enzymes that support protein trafficking and post-translational modifications (reviewed in Ref. 3). Excess Mn^{2+} intake leads to manganism, a Parkinson-like disease that affects miners, welders, steel, and battery workers due to Mn^{2+} intoxication (4), and SPCA1 may play a role in Mn^{2+} detoxification in the liver (5).

Most eukaryotes express a single SPCA orthologue, which is called plasma membrane-related Ca^{2+}-ATPase 1 (PMR1). In tetrapods, two isoforms are found, SPCA1 and SPCA2, which share 63% sequence identity and 73% similarity. The human isoform SPCA1 is ubiquitously expressed from the *ATP2C1* gene. Haplo-insufficiency of SPCA1 leads to Hailey–Hailey disease, an autosomal dominant skin disorder characterized by loss of cell–cell adhesion (6). The second human isoform, SPCA2, is encoded by the *ATP2C2* gene and SPCA2 protein expression is constrained to brain, testis, and actively secreting cells, such as mammary gland epithelial cells, suggesting a more specialized function (7–10).

The two human SPCA isoforms activate the plasma membrane Ca^{2+} channel Orai1, which is referred to as store-independent Ca^{2+} entry (SICE) (11, 12). Although store-operated Ca^{2+} entry (SOCE) relies on the depletion of the endoplasmic reticulum Ca^{2+} store that triggers STIM1-mediated Orai1 acti-

This work was supported by Flanders Research Foundation FWO Grants G044212N and G0B1115N (to P. V.) and Inter-University Attraction Poles program P7/13. The authors declare that they have no conflicts of interest with the contents of this article.
This article contains Figs. S1–S6.

[1] Strategic Basic Research Ph.D. fellow at FWO supported by Grant 1S23217N.

[2] To whom correspondence should be addressed: ON1 Campus Gasthuisberg, KU Leuven Herestraat 49/box 802, B3000 Leuven, Belgium. Tel: 32-16-330720; E-mail: peter.vangheluwe@kuleuven.be.

[3] The abbreviations used are: SERCA, sarco(endo)plasmic reticulum Ca^{2+}-ATPase; SPCA, secretory pathway Ca^{2+}-ATPase; PMCA, plasma membrane Ca^{2+}-ATPase; PMR1, plasma membrane-related Ca^{2+}-ATPase 1; SICE, store-independent Ca^{2+} entry; SOCE, store-operated Ca^{2+} entry; HA, hydroxylamine; GST, glutathione *S*-transferase; HSQC, heteronuclear single quantum coherence; BisTris, 2-[bis(2-hydroxyethyl)amino]-2-(hydroxymethyl)propane-1,3-diol; TES, 2-{[2-hydroxy-1,1-bis(hydroxymethyl)ethyl]amino}ethanesulfonic acid; ANOVA, analysis of variance; AA, double alanine mutant.

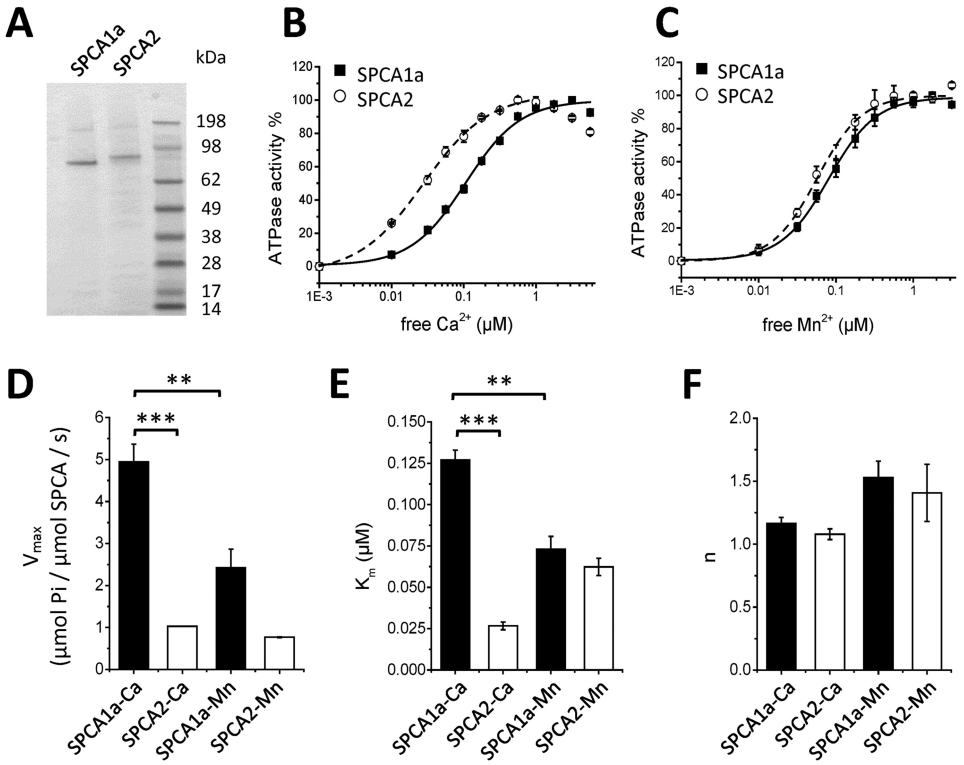

Figure 1. ATPase activity of reconstituted SPCA1a and SPCA2. *A,* a Coomassie-stained SDS-PAGE gel displays purified and reconstituted SPCA1a and SPCA2 proteins. The SeeBlue Plus2 was used as molecular weight marker. Ca^{2+} (*B*) and Mn^{2+} (*C*)- dependent ATPase activities measured on reconstituted SPCA1a (*filled squares*) and SPCA2 (*empty circles*) were normalized to their maximal activities, and fitted with logistic functions. *D–F,* bar graphs depicting the parameters of the maximal ATPase activity (V_{max}, *D*), apparent affinities (K_m, *E*) and cooperativities (*n*, *F*) for Ca^{2+} and Mn^{2+} were derived from *B* and *C* ($n = 3–5$).

vation, SICE leads to Ca^{2+} entry through the Orai1 channel independently of STIM1 (11, 12). The incoming Ca^{2+} in cells is subsequently transferred to the secretory pathway (12, 13). Because both SPCA1 and SPCA2 are up-regulated in the mammary gland during lactation, SICE may promote cellular Ca^{2+} uptake for subsequent secretion in the milk via the secretory pathway (14, 15). In addition, SICE is chronically activated by SPCA2 in luminal-type breast cancer cells, which causes Ca^{2+} dyshomeostasis and aberrant cell proliferation (11). SPCA1 is implicated in the basal-type breast cancer (16, 17), whereas up-regulation of both SPCA genes is associated with microcalcifications during breast cancer (16).

Structures of the SERCA1a Ca^{2+} pump were solved in the main catalytic states providing detailed insights into its Ca^{2+} transport mechanism and domain architecture, which seems to be highly conserved between Ca^{2+}-ATPases (18, 19). But compared with SERCA1a, the PMCA and SPCA pumps contain longer N- and C-terminal extensions, which presumably act as regulatory elements. The C terminus of PMCA clearly serves as an autoinhibitory domain that is regulated by calmodulin, protein kinases, and lipids (20). The functional role of the N or C termini of SPCA isoforms is also gradually emerging. Truncations of the SPCA2 N and C termini functionally impair SPCA2 (12). Moreover, a motif in the N terminus of SPCA2 controls the binding to Orai1 (11), whereas at the corresponding position of the *Saccharomyces cerevisiae* orthologue PMR1, a Ca^{2+}-binding EF-hand–like motif is found, which is important for ion selectivity (21). Of interest, the ion selectivity of the yeast PMR1 protein to Ca^{2+} and Mn^{2+} depends on this N-terminal element (21), although other residues in the TM region are also important (22).

In this study, we directly compared the functional properties of the purified SPCA1a and SPCA2 protein in reconstituted proteoliposomes and discovered unexpected isoform-specific differences in Ca^{2+} *versus* Mn^{2+} affinities and turnover rates. These differences depend at least in part on a Ca^{2+}-binding EF-hand–like motif in the SPCA1a N terminus that is absent in SPCA2.

Results

Purified SPCA1a and SPCA2 present different Ca^{2+}-, but not Mn^{2+}-dependent activities

To functionally compare the SPCA1a and SPCA2 isoforms, we purified both isoforms and reconstituted them in proteoliposomes following the same procedure as we described before for SPCA1a (23). In short, the human His-tagged SPCA1a or SPCA2 isoforms were expressed in *S. cerevisiae*, affinity purified from solubilized membrane fractions, and then incorporated into lipid vesicles (Fig. 1*A*). The His_{10}-tagged SPCA2 monomer (105.9 kDa) ran at a slightly higher position on SDS-PAGE than the His_8-tagged SPCA1a (101.8 kDa), matching their predicted molecular masses. To compare the functional properties of the reconstituted SPCA1a and SPCA2 isoforms, we evaluated the Ca^{2+}- (Fig. 1*B*) or Mn^{2+}-dependent (Fig. 1*C*) ATPase activities with a colorimetric method to detect P_i levels (24), and observed remarkable isoform-specific differences. SPCA1a displays a 2-fold higher Ca^{2+}-dependent maximal ATPase activity

Table 1
Summary of parameters obtained from the ATPase assay

	K_m	n	V_{max}
	μM		μmol P_i/μmol SPCA/s
SPCA1a-Ca	0.13 ± 0.01	1.17 ± 0.05	4.94 ± 0.42
SPCA2-Ca	0.03 ± 0.00	1.08 ± 0.04	1.03 ± 0.01
SPCA1a-Mn	0.07 ± 0.01	1.53 ± 0.13	2.43 ± 0.44
SPCA2-Mn	0.06 ± 0.01	1.41 ± 0.23	0.77 ± 0.01

(V_{max}) as compared with Mn^{2+}, whereas SPCA2 presents a similar V_{max} for both substrates (Fig. 1*D*). SPCA1a also exhibits a lower affinity for Ca^{2+} than for Mn^{2+}, whereas this is opposite for SPCA2 (Fig. 1*E*). The cooperativity (n) of both enzymes for Ca^{2+} approximates 1, confirming that one Ca^{2+} is transported per ATP. The cooperativity of both isoforms toward Mn^{2+} is slightly, but not significantly higher (Fig. 1*F*). In conclusion, SPCA1a presents similar properties as SPCA2 in Mn^{2+} conditions, but a higher V_{max} and lower apparent affinity in Ca^{2+} conditions (Table 1, Fig. 1, *B–E*).

SPCA1a, but not SPCA2, autophosphorylation presents a biphasic activation pattern

Like other P-type ATPases, SPCA isoforms catalyze a substrate-dependent autophosphorylation reaction on a conserved Asp residue in the phosphorylation domain (3, 25). We here confirm that the reconstituted SPCA isoforms form Ca^{2+}- or Mn^{2+}-dependent phospho-enzyme (EP) intermediates when incubated with radiolabeled ATP (Fig. 2, *A* and *B*). Note that a batch-dependent background phosphorylation was sometimes detected in the EGTA conditions, which most likely represents another low abundant phosphorylated protein that runs higher than SPCA1a. Because SPCA2 is slightly larger than SPCA1, this background signal runs at the same height as SPCA2, making it impossible to separate both phosphorylation signals. Because this additional signal is Ca^{2+}- and Mn^{2+}-independent, we subtracted it as background from the Ca^{2+}- or Mn^{2+}-dependent EP levels that represent the SPCA activity.

Interestingly, we observed a remarkable difference between the Ca^{2+}-dependent autophosphorylation behavior of both isoforms (Fig. 2, *A* and *C*). SPCA2 reached maximal autophosphorylation already at low micromolar free Ca^{2+}, whereas the SPCA1a EP level raised further above 3 μM and reached a maximum at 3 mM free Ca^{2+}, *i.e.* well above the physiological Ca^{2+} concentrations in the cytosol. Thus, the difference between the apparent Ca^{2+} affinities of SPCA1a and SPCA2 is much more pronounced in the EP assay (Table 2) than in the ATPase assay (Fig. 1 and Table 1). This most likely relates to the difference in ATP concentration between both assays (5 mM ATP in ATPase assay, *versus* 5 μM cold and radiolabeled ATP in the autophosphorylation assay). Indeed, increasing the ATP concentration from 5 to 50 μM shifts the SPCA1a EP curve to higher affinity, whereas reducing the ATP to 0.5 μM lowers the Ca^{2+} affinity (Fig. S1*A*). Conversely, decreasing the ATP concentration from 5 mM to 500 μM in an enzyme-coupled ATPase assay (which ensures that ATP is not depleted) also lowers the Ca^{2+} affinity of SPCA1a (Fig. S1*B*). This highlights that the Ca^{2+} affinity of SPCA1a is highly sensitive to the available ATP concentration. Moreover, the apparent Ca^{2+} affinity of SPCA1a autophosphorylation would be considerably higher at physiological ATP concentrations, *i.e.* more in line with the ATPase assay.

A similar EP pattern is observed in Mn^{2+} conditions (Fig. 2, *B* and *D*). SPCA2 already reached a maximal EP level in the presence of 0.3 μM free Mn^{2+}, in line with a very high apparent Mn^{2+} affinity of SPCA2, whereas SPCA1a displayed a biphasic stimulation by Mn^{2+}. The first part of the curve plateaus at ~3 μM Mn^{2+}, when ~60% of the maximal EP level is reached (Fig. 2*D*). The second part of the curve rises from ~30 μM Mn^{2+} onwards, and the maximal EP level is obtained around 1 mM. Like for the ATPase activities, both SPCA1a and SPCA2 present n values higher than 1 in Mn^{2+}-induced phosphorylation, indicating positive cooperativities (Table 2). However, SPCA1a's cooperativity toward Ca^{2+} is lower than one.

Inspired by the biphasic profile of the Mn^{2+}-dependent EP formation results, we carefully re-analyzed the results of the Ca^{2+}-dependent EP assays and fitted a biphasic instead of a mono-sigmoidal curve in the data presented in Fig. 2*C*. Fitting with two logistic curves that are separated at 30 μM Ca^{2+} rendered an SPCA1a cooperativity for both the first and second phases of $n = 1$ (Fig. 2*E*, Table 2), suggesting that this may represent a better fit of the data. However, the biphasic pattern is not observed in ATPase measurements at 5 mM ATP, because at high Ca^{2+} or Mn^{2+} concentrations (*i.e.* above 10 μM) the ATPase activity of both isoforms decreases, which is known as back-inhibition of the pump (Fig. S2, *A* and *B*). However, once the ATP concentration in the ATPase assay is lowered to 0.5 mM, we found that SPCA1a also displayed a biphasic activation profile in the physiological Ca^{2+} concentration range (above 1 μM Ca^{2+}) (Fig. S3). We therefore conclude that at low ATP concentration SPCA1a presents an unusual biphasic activation behavior, which may point to an autoregulatory mechanism that controls SPCA1a's activity and substrate affinity and is sensitive to the ATP concentration.

The efficacy of SPCA1a's autophosphorylation is higher with Ca^{2+} than Mn^{2+}

SPCA proteins transport Ca^{2+} and Mn^{2+} via the same ion-binding pocket in the transmembrane domain (26). Because binding of Mn^{2+} or Ca^{2+} at this binding pocket causes EP formation, we anticipated that saturating Ca^{2+}/Mn^{2+} concentrations (3 μM for SPCA2 or 3 mM for SPCA1a) should yield similar EP levels for each isoform. To verify this, we directly compared the EP levels of both isoforms at 3 μM and 3 mM Ca^{2+} or Mn^{2+}. As predicted, we observed that the SPCA2 EP levels were comparable at saturating concentrations of Ca^{2+} or Mn^{2+} (3 μM). No stimulation of EP levels was observed at higher Ca^{2+} or Mn^{2+} concentrations (Fig. 3, *A* and *B*). Although the EP level at 3 μM Ca^{2+} or Mn^{2+} was also similar for SPCA1a, the maximal EP level at 3 mM Ca^{2+} was 4.2-fold higher than at 3 mM Mn^{2+} (Fig. 3, *A* and *B*), which indicates that the autophosphorylation reaction of SPCA1a is more stimulated by Ca^{2+} than Mn^{2+}. To further test the ion specificity of this EP stimulation, we compared normal (5 mM) *versus* higher (8 mM) Mg^{2+} concentrations. Mg^{2+} is an essential divalent ion that is included in the assay at 5 mM to support the ATP coordination and autophosphorylation reaction. However, Mg^{2+} ions, in the absence of Ca^{2+} or Mn^{2+}, did not induce any EP formation of the SPCA

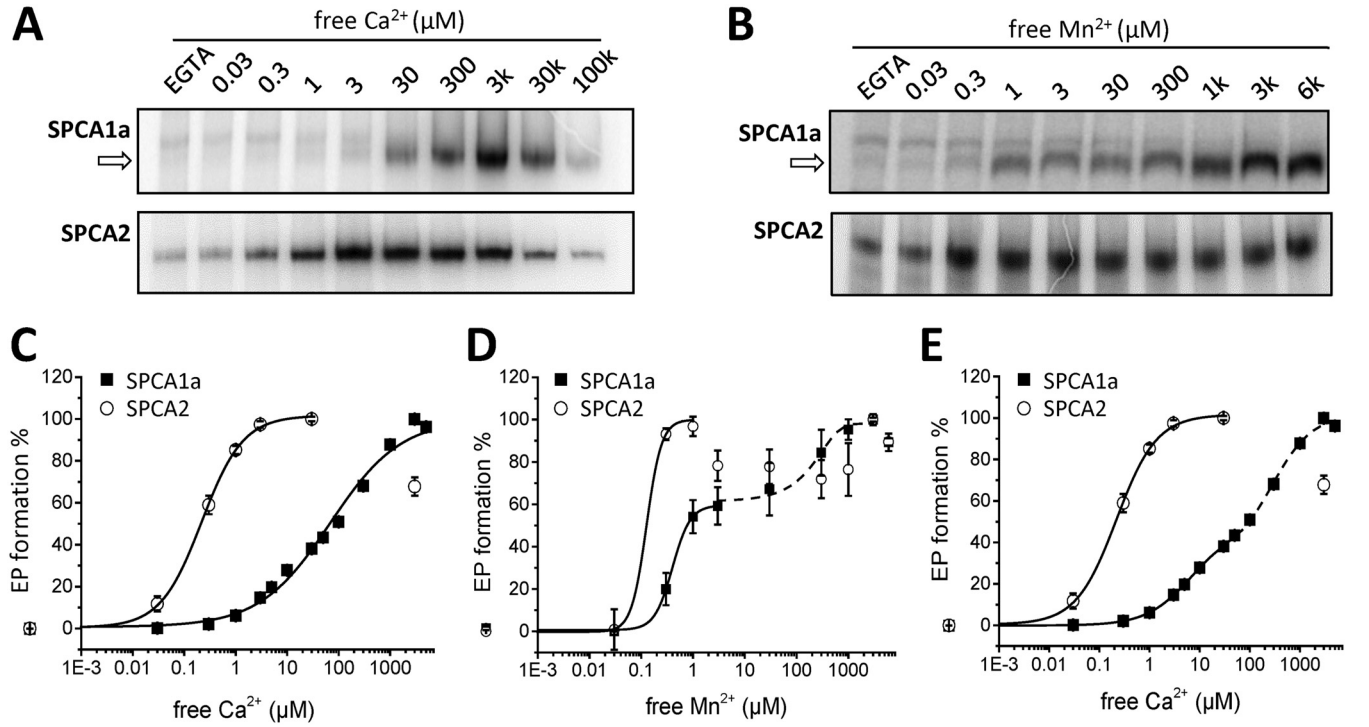

Figure 2. Autophosphorylation of reconstituted SPCA1a and SPCA2. *A* and *B*, phosphorimages depict the radiolabeled SPCA1a (*upper*) and SPCA2 (*lower*) phospho-intermediates (EP) at various Ca^{2+} (*A*) or Mn^{2+} (*B*) concentrations, separated by gel electrophoresis. The *arrows* indicate the Ca^{2+}- or Mn^{2+}-sensitive phosphorylated SPCA1a bands. The radioactivity was quantified with ImageJ software and the EGTA signal was subtracted as background. *C* and *D*, radioactivity was used as a measure of EP formation, which was plotted in a Ca^{2+} (*C*)- or Mn^{2+} (*D*)-dependent manner and was fitted with logistic functions. The SPCA1a Mn^{2+}-dependent autophosphorylation curve was fitted with two consecutive logistic functions, revealing a biphasic activation curve. *E*, re-fitting of the SPCA1a Ca^{2+}-dependent autophosphorylation data in *C* with two consecutive logistic functions, revealing a biphasic activation pattern (n = 3–7).

Table 2

Summary of parameters obtained from the autophosphorylation assay of SPCA1 and SPCA2

	K_m	n	Fitting
	μM		
SPCA1a-Ca	68.5 ± 10.4	0.63 ± 0.05	Monophasic
	7.9 ± 0.1	0.95 ± 0.03	Biphasic part I
	294.0 ± 51.0	1.14 ± 0.27	Biphasic part II
SPCA2-Ca	0.22 ± 0.01	1.08 ± 0.07	Monophasic
SPCA1a-Mn	0.43 ± 0.03	1.89 ± 0.32	Biphasic part I
	103.2 ± 52.4	0.004 ± 0.001	Biphasic part II
SPCA2-Mn	0.13 ± 0.05	2.99 ± 1.38	Monophasic

isoforms (Fig. 3, *A* and *B*), indicating that only Ca^{2+} is able to maximally activate SPCA1a autophosphorylation.

The maximal EP levels observed at 3 μM Ca^{2+} for SPCA2 and 3 mM Ca^{2+} for SPCA1a reflect the active protein fractions, which can be used to determine the maximal turnover rates. The ratio between the maximal ATPase activity (nmol of P_i released/μg of protein/s) and the maximal level of autophosphorylated protein (nmol of protein phosphorylated/μg of protein) is typically used to calculate the maximal turnover rates of Ca^{2+} transport ATPases (s^{-1}), as described before (27–29). The maximal turnover rate of SPCA1a is almost twice as high with Ca^{2+} than with Mn^{2+}, or as compared with SPCA2 (Fig. 3*C*). For SPCA2, the maximal turnover rates are similar with Mn^{2+} or Ca^{2+} (Fig. 3*C*).

Next, we verified that the second activation step of the SPCA1a autophosphorylation represents the catalytic autophosphorylation of the conserved Asp residue. It is possible that the second activation step may be caused by a low abundant kinase that promotes phosphorylation of SPCA1a on a Ser/Thr/Tyr acceptor site. To discriminate between both possibilities, we administered hydroxylamine (HA) to the phosphoenzymes, which specifically quenches acyl phosphates on the Asp, but is not reactive to phospho-Ser/Thr/Tyr residues (30). HA treatment completely abolished the Ca^{2+}-dependent phosphorylation signal of SPCA1a and SPCA2, confirming that the EP levels represent aspartyl phosphorylation at the catalytic autophosphorylation site (Fig. 3, *D* and *E*). In contrast, HA treatment did not quench the Ca^{2+}-insensitive background phosphorylation signal, confirming that it occurs independently of the autophosphorylation reaction, most likely on an unrelated trace protein (Fig. 3, *D* and *E*). Together, only Ca^{2+} is able to maximally activate catalytic SPCA1a autophosphorylation, which may point to a Ca^{2+}-dependent regulation mechanism of SPCA1a.

Only in SPCA1a, Ca^{2+} is able to replace Mg^{2+} to induce autophosphorylation

We hypothesized that the strongest stimulation of SPCA1a autophosphorylation by Ca^{2+} and the two-step activation pattern may be explained by a regulatory Ca^{2+}-binding site that is only present in SPCA1a and not in SPCA2. The presence of such an ion-binding element is supported by the observation that high concentrations of Ca^{2+} result in a mobility shift of the SPCA1a monomer on native PAGE (Fig. 4*A*). The sharp SPCA1a monomer band that is observed in the EGTA condition becomes more diffuse and migrates at a higher part of the gel when 3 mM Ca^{2+} is supplied (*box* in Fig. 4*A*). This behavior is less pronounced with 3 μM Ca^{2+} or 3 μM/3 mM Mn^{2+} (Fig.

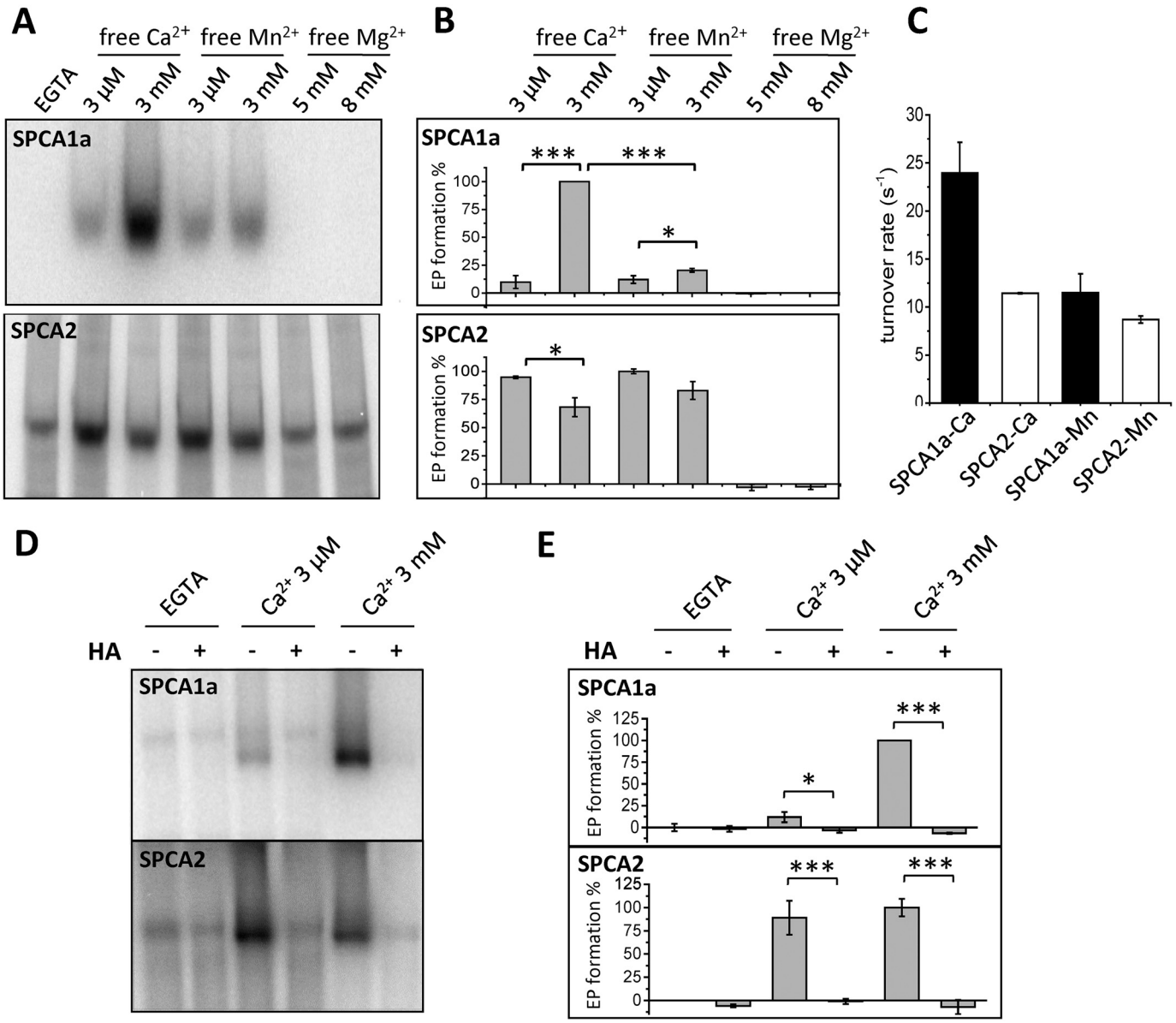

Figure 3. Comparison of the Ca^{2+}-, Mn^{2+}-, or Mg^{2+}-induced autophosphorylation in SPCA1a and SPCA2. *A,* phosphorimages of the radiolabeled SPCA1a (*upper*) and SPCA2 (*lower*) phospho-intermediates (EP) separated by gel electrophoresis. Indicated concentrations of Mn^{2+} or Ca^{2+} were supplied in the presence of 5 mM $MgCl_2$. In the Mg^{2+} conditions, only 5 or 8 mM $MgCl_2$ was administered. *B,* bar graphs depicting the EP levels in various conditions. The radioactivity was quantified with ImageJ software and the EGTA signal was subtracted as background. *C,* bar graph depicting the turnover rates of both isoforms. Turnover rates were calculated by dividing the maximal ATPase activities over the maximal phosphorylation activities ($n = 3$). *D,* representative phosphorimages of SPCA1a or SPCA2 treated with radiolabeled ATP followed by administration of HA, a quencher of aspartyl-phosphate intermediates. Experiments were conducted in the presence of EGTA, 3 μM or 3 mM Ca^{2+} ($n = 3$). *E,* quantification of radioactivity in *D* was performed using ImageJ software. One-way ANOVA was performed followed by post hoc Bonferroni test. *, $p < 0.05$; **, $p < 0.01$; ***, $p < 0.001$.

4*A*). Note that we also observed SPCA1a dimers on native PAGE, which were less influenced by Ca^{2+} binding (presumably due to the low resolution of the separation of larger protein complexes in gradient gels). The addition of Ca^{2+} had no effect on the SPCA1a monomer/dimer ratio (Fig. 4*B*). Furthermore, no mobility shift of the monomer band was observed for SPCA2 and SERCA1a at 3 μM or 3 mM Ca^{2+}, although the monomer/dimer ratio was altered (Fig. S4). Together this indicates that the Ca^{2+}-induced mobility shift of the monomer is an SPCA1a-specific behavior, which may be due to changes in charge, mass, and/or conformation of SPCA1a caused by the binding of Ca^{2+}. Because the mobility shift was less pronounced with Mn^{2+}, this indicates that the regulatory binding site of Ca^{2+} may differ from the Ca^{2+}/Mn^{2+}-binding site for transport in the transmembrane region.

As a first possibility for a regulatory divalent cation-binding site, we considered the conserved Mg^{2+}-binding site near the ATP-binding site that is present in all P-type ATPases. It is known that high Mn^{2+} levels interfere with Mg^{2+} binding in proteins (31, 32). We therefore reasoned that by competing with Mg^{2+} at this site, the millimolar concentrations of Ca^{2+} or Mn^{2+} may affect the ATP coordination and autophosphorylation reaction of SPCA1a in a different way than SPCA2. We therefore tested if the elevated EP level in SPCA1a may be

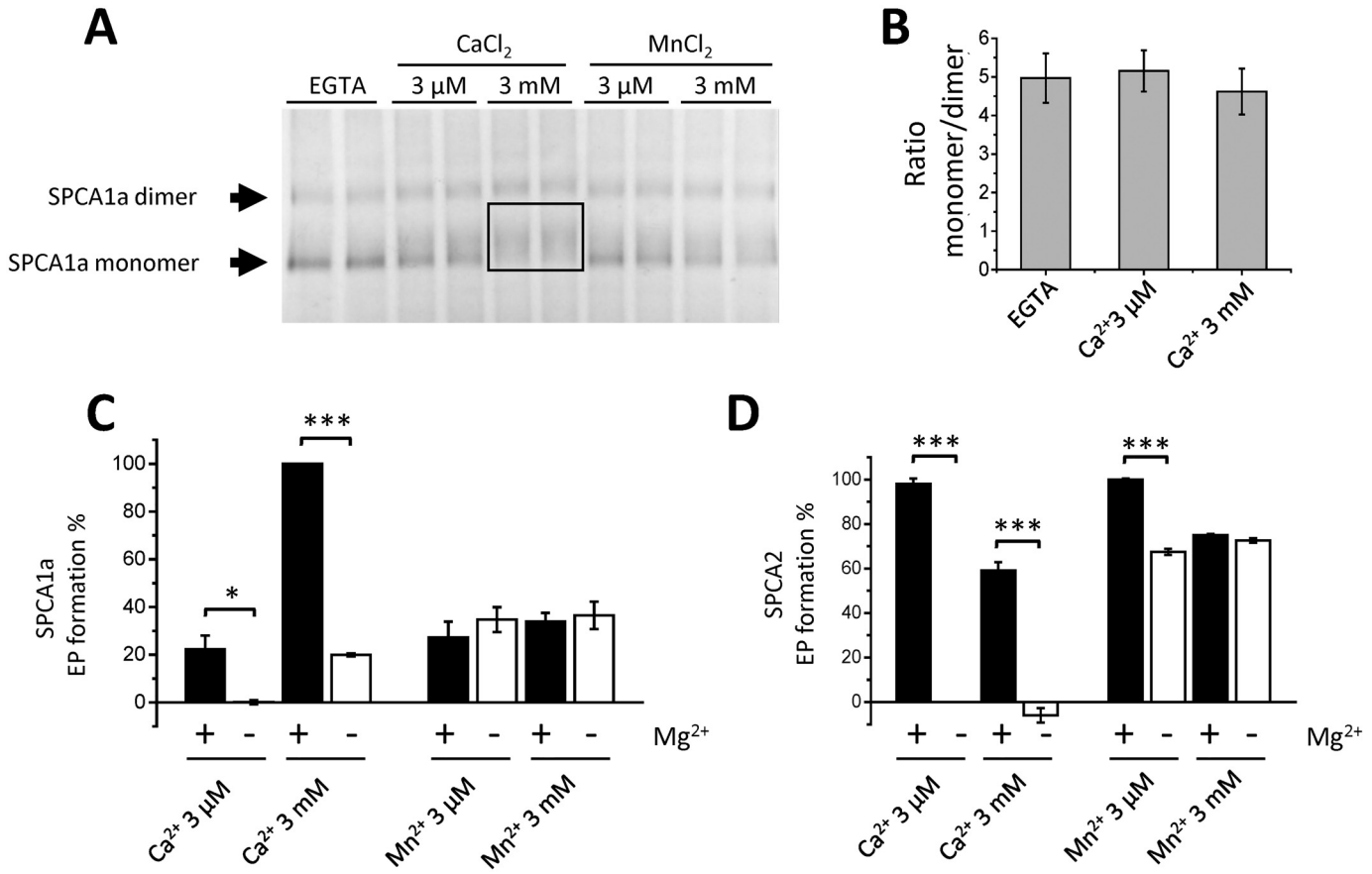

Figure 4. Binding of Ca^{2+} and Mn^{2+} to SPCA proteins. *A,* native PAGE of purified SPCA1a protein following incubation with varying concentrations of Ca^{2+} or Mn^{2+}. Bands were visualized by Coomassie staining. The *arrows* point to the SPCA1a monomer and dimer bands in the EGTA condition. The monomer protein band appears less focused in the presence of 3 μM Ca^{2+} and migrates higher as a smear in the 3 mM Ca^{2+} condition (*boxed region*). *B,* quantified monomer/dimer band ratio of the SPCA1a in Native PAGE ($n = 7$). *C* and *D,* bar graphs depicting the quantified EP levels of SPCA1a (*C*) and SPCA2 (*D*). Indicated concentrations of Mn^{2+} or Ca^{2+} were supplied in the presence (5 mM) or absence (0 mM) of $MgCl_2$ ($n = 2$). The EP levels were normalized to the maximal level of each isoform. *, $p < 0.05$; **, $p < 0.01$; ***, $p < 0.001$.

explained by the competition between Mg^{2+} and Ca^{2+} or Mn^{2+} (Fig. 4, *C* and *D*). Both SPCA1a and SPCA2 largely retained high EP levels when 5 mM Mg^{2+} was replaced by 3 μM or 3 mM Mn^{2+} (Fig. 4, *C* and *D*), indicating that Mn^{2+} is able to substitute for Mg^{2+} in both isoforms. In contrast, in the absence of Mg^{2+}, 3 μM or 3 mM Ca^{2+} is unable to induce EP formation in SPCA2 (Fig. 4*D*). Remarkably, EP formation is observed for SPCA1a when 3 mM Ca^{2+} is used, albeit significantly lower (19.3%) than when Mg^{2+} is present (100.0%) (Fig. 4*C*).

Thus, SPCA2 can be autophosphorylated with Mg^{2+} or Mn^{2+} as ATP coordinating ions, whereas SPCA1a is also able to use Ca^{2+} for ATP coordination and autophosphorylation. However, Ca^{2+} is 4-fold less efficient to induce autophosphorylation in the absence of Mg^{2+}. Because the strong stimulatory effect of millimolar Ca^{2+} on the SPCA1a autophosphorylation depends on the presence of Mg^{2+} (Fig. 4*C*), we hypothesized that another SPCA1a-specific region than the Mg^{2+}-binding site may be responsible.

The N terminus of SPCA1a, but not SPCA2, contains a Ca^{2+}-binding site

Yeast PMR1 possesses a Ca^{2+}-binding EF-hand–like motif in its N terminus, which determines substrate selectivity and pumping activity (21). This motif is partially conserved in SPCA1a sequences of higher vertebrates (Fig. 5*A*), but the loop of the EF-hand–like motif of PMR1 comprises one extra amino acid. The critical acidic residues at positions Asp-51, Asp-53, and Glu-63 of the motif in PMR1 are reasonably conserved in SPCA1a (Gln-39, Asp-41, and Glu-50), but less conserved in SPCA2 (Cys-70, Asp-72, and Ser-81) or in invertebrate PMR1 sequences. Based on this alignment, we hypothesized that the N-terminal region of SPCA1a may hold a Ca^{2+}-binding motif that may explain the Ca^{2+}-dependent stimulation of SPCA1a's autophosphorylation activity.

We turned to an NMR analysis of the human SPCA1a N terminus to pinpoint residues that may contribute to Ca^{2+} binding. We first purified a GST-labeled N-terminal SPCA1 fragment and removed the GST tag via thrombin cleavage. This rendered a >95% pure protein fragment corresponding to Val-20 to Glu-67 of SPCA1a (Fig. 5*B*), which was suitable for NMR analysis. This purified peptide was analyzed in the absence and presence of Ca^{2+} using NMR spectroscopy (Fig. 5*C*). Based on the chemical shift changes of backbone amide signals in ^{15}N-HSQC spectra at different titration steps, we were able to unambiguously identify a stretch of residues that are significantly affected at their backbone by Ca^{2+} binding:

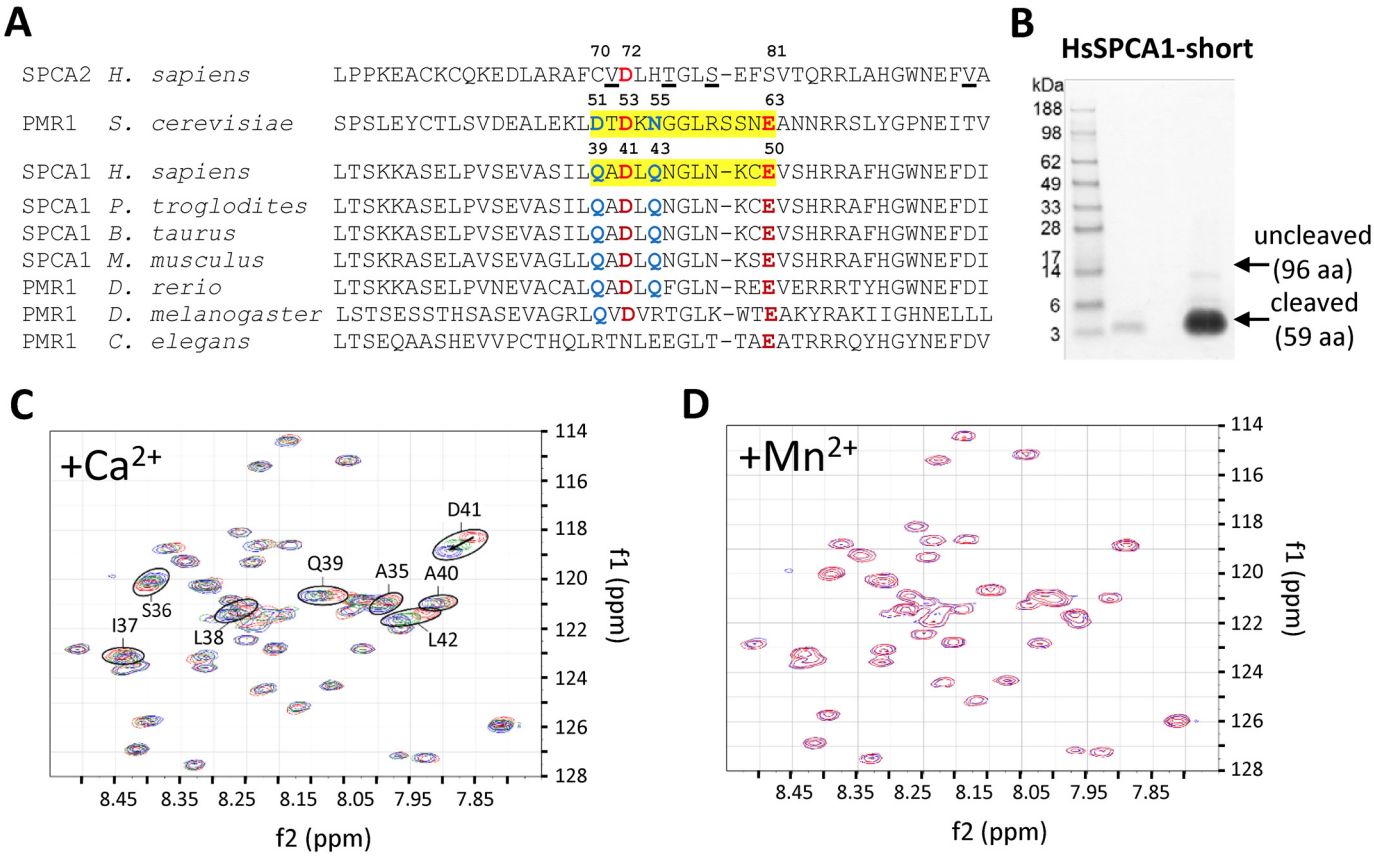

Figure 5. Binding of Ca^{2+} to the N-terminal EF-hand–like motif in SPCA1a. *A,* MUSCLE alignment of part of the N-terminal sequences of yeast PMR1 (NP_011348.1), human SPCA1 (NP_001186110.1), and SPCA2 (B4E2Q0), with various animal SPCA1/PMR1 orthologues (XP_001146246.2; NP_786979.1; NP_001240760.1; XP_003200287.2; NP_730742.1; NP_001021862.1). The regions highlighted in *yellow* in yeast PMR1 and human SPCA1 correspond to the loop of the EF-hand–like motif. The critical residues that are identical (*red*) or conserved (*blue*) between yeast PMR1 and human SPCA1 are indicated with numbering. In SPCA2, the *underlined* residues interact with Orai1 during store-independent Ca^{2+} entry (11). *B,* Coomassie staining of purified N-terminal fragment of SPCA1a (including an N-terminal linker SPMGYRGSM followed by the human SPCA1a sequence Val-20 to Glu-67). *C,* the heteronuclear single quantum coherence spectra overlay of the SPCA1a N-terminal peptide purified from *B* in the presence of 0 (*red*), 4.65 (*green*), and 9 mM (*blue*) Ca^{2+} ions. *Encircled* residues with the indicated numbers were identified in close vicinity of a Ca^{2+} ion. *D,* overlay of heteronuclear single quantum coherence spectra before (*blue*) and after (*red*) further addition of Mn^{2+} after the Ca^{2+} titration.

Ser-36 to Leu-42 (Fig. 5*C*). The observed chemical shift changes can be attributed to direct interaction with Ca^{2+} or local conformational changes upon Ca^{2+} binding (33). The identified region contains Gln-39 and Asp-41, which are conserved residues in the EF-hand–like motif of PMR1 and SPCA1a (Fig. 5*A*).

After titrating with $CaCl_2$, we also added $MnSO_4$ as a competition experiment. Strong impact on protein signals upon binding Mn^{2+} is expected because its unpaired electron induces paramagnetic relaxation effects on NMR active nuclei within a distance of about 15 Å. Therefore, binding of the peptide with Mn^{2+} would result in line broadening and potentially removing signals from the NMR spectra (34). To avoid this problem and to potentially allow a second titration, the amount of Mn^{2+} added was an order of magnitude smaller than the added amount of Ca^{2+} but should still suffice to establish any influence (binding) of Mn^{2+} to the peptide. The absence of any observable changes in NMR spectra after the addition of $MnSO_4$ indicates that this N-terminal peptide of SPCA1a does not bind Mn^{2+} (Fig. 5*D*). Together, our data show that SPCA1a harbors a Ca^{2+}-selective EF-hand–like motif in its N terminus.

The N-terminal EF-hand–like motif provides Ca^{2+} specific control of SPCA1a activity

Next, we explored whether the N-terminal EF-hand–like motif of SPCA1a is responsible for the Ca^{2+}-specific activation mechanism of autophosphorylation. We performed site-directed mutagenesis to disturb the motif, and generated two single mutants, Q39C and E50S, in which SPCA1a residues are substituted by the corresponding SPCA2 residues. Because SPCA2 may not bind Ca^{2+} at the N terminus (Fig. S4), we hypothesize that by introducing SPCA2 elements, we will affect the 3D configuration of the EF-hand–like motif and compromise Ca^{2+} coordination. Note also that Glu-50 is a highly conserved acidic residue in the canonical EF-hand sequences (35). Finally, we constructed a double mutant in which the two conserved acidic residues between SPCA1 and PMR1 are replaced by alanines (D41A/E50A). The three SPCA1a mutants were purified and reconstituted following the same procedure as for WT (Fig. 6*A*). Interestingly, the Ca^{2+}-dependent mobility shifts of the mutant proteins are less prominent as compared with the purified WT protein, indicating that Ca^{2+} binding is hampered by the EF-hand mutations (Fig. 6*B*).

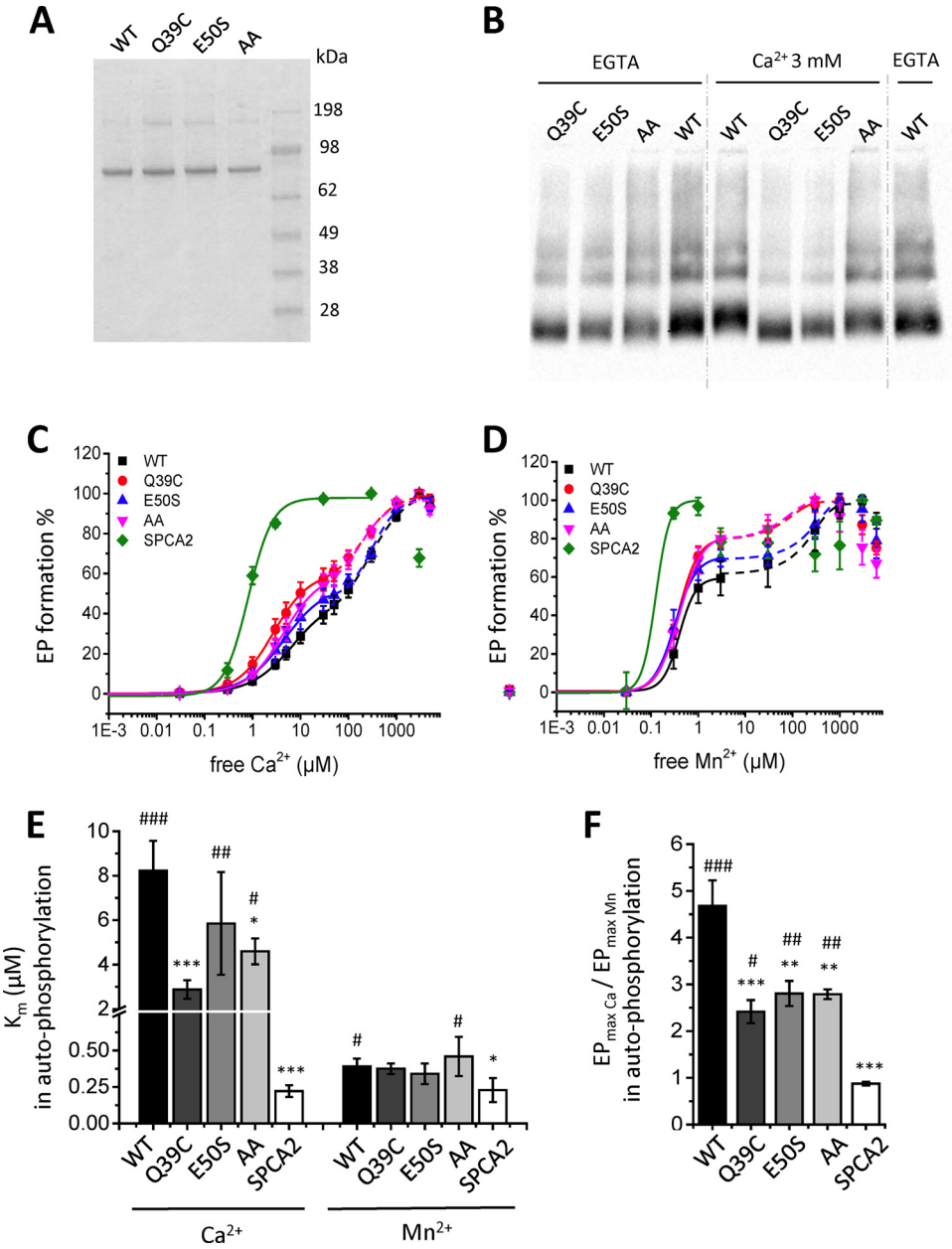

Figure 6. Autophosphorylation activities of SPCA1a WT and N-terminal EF-hand–like mutants. *A*, a Coomassie-stained SDS-PAGE gel of the reconstituted SPCA1a WT and mutants. *B*, native PAGE of the SPCA1a WT and mutants incubated with or without Ca^{2+}, followed by immunoblotting for detection with a SPCA1-specific antibody (1:50,000 dilution, Frodo, homemade). *C* and *D*, Ca^{2+}- and Mn^{2+}-dependent autophosphorylation activities were measured from radiograms for all constructs, and fitted with either one (for SPCA2) or two (for SPCA1a and the mutants) logistic curves (n = 3–7). Bar graphs depict the apparent ion affinities of the first phase (K_m, *E*) and the ratio of the maximal phosphorylation levels of Ca^{2+} over Mn^{2+} (*F*), which were derived from the measurements by fitting of each individual measurement, shown in *B* and *C*. One-way ANOVA was performed followed by post hoc Fisher (*E*) and Bonferroni (*F*) tests. *, significantly different compared with SPCA1a WT. #, significantly different compared with SPCA2. *, $p < 0.05$; **, $p < 0.01$; ***, $p < 0.001$. AA, double alanine mutant.

Remarkably, the biphasic pattern of the Ca^{2+}-dependent autophosphorylation at 5 μM ATP is more pronounced for the SPCA1a mutants than for WT (Fig. 6*B*), which further shows that our earlier formulated proposal for a biphasic fitting of the Ca^{2+}-dependent autophosphorylation of WT is justified (Fig. 2*E*). The mutants Q39C and AA displayed a significantly higher Ca^{2+} affinity in the first activation phase of Ca^{2+}-dependent autophosphorylation, whereas the affinity shift for E50S is more modest (Fig. 6, *C* and *E*, Table 3). In ATPase assays in the presence of 5 mM ATP, all mutants exhibited a significantly higher apparent affinity for Ca^{2+}, *i.e.* shifting the K_m value closer to SPCA2's K_m (Fig. 7, *A* and *C*). A more modest effect of the mutations was observed on the apparent Mn^{2+} affinity (Figs. 6, *D* and *E*, and 7, *A*–*C*, Table 3). Thus, we show that the EF-hand–like motif mainly regulates the apparent Ca^{2+} affinity of SPCA1a, but has a lower impact on Mn^{2+} affinity, which is in line with the selectivity of the EF-hand–like motif for Ca^{2+} over Mn^{2+} (Fig. 5, *C* and *D*).

Moreover, the EF-hand–like motif also plays a role in the biphasic activation pattern of SPCA1a (Fig. 6, *C* and *D*). Indeed, the relative magnitudes of the second phosphorylation phase were reduced in all three mutants (Fig. 6, *C* and *D*). The appar-

Table 3
The affinity of Ca^{2+} and Mn^{2+} obtained from autophosphorylation assay of SPCA1 mutants

	K_m, biphasic part I[a]	K_m, biphasic part II[b]
	μM	
WT-Ca	7.9 ± 0.1	285
Q39C-Ca	2.8 ± 0.1	204
E50S-Ca	4.6 ± 0.4	373
AA-Ca	4.4 ± 0.1	189
WT-Mn	0.43 ± 0.03	242
Q39C-Mn	0.37 ± 0.02	78
E50S-Mn	0.32 ± 0.01	259
AA-Mn	0.40 ± 0.02	73

[a] The K_m of biphasic part I is calculated from the overall fitting of $n = 3$–7 curves via logistic function in Origin Pro9.
[b] K_m of biphasic part II is calculated by enabling "finding x from y" function in Origin Pro 9. The y values are determined with formula, $100 - 0.5 \times (100 - A1)$, A1 is the starting y value of the biphasic part II.

ent Ca^{2+} and Mn^{2+} affinity of the second phase was higher for the Q39C and AA mutants as compared with E50S and WT (Fig. 6, *C* and *D*, Table 3). However, the ratio of the maximal EP levels obtained in Ca^{2+} over Mn^{2+} ($EP_{max(Ca)}/EP_{max(Mn)}$) shows that the three mutants became less responsive to Ca^{2+} relative to Mn^{2+} (Fig. 6*F*). In addition, we confirmed in ATPase measurements that the single mutants displayed a lower $V_{max(Ca)}/V_{max(Mn)}$ ratio, more closely resembling SPCA2 (Fig. 7*D*). Thus, these results reveal that the EF-hand–like motif contributes to the Ca^{2+}-specific activation of autophosphorylation in SPCA1a, which regulates the maximal Ca^{2+}-dependent ATPase activity.

Also the maximal ATPase activity of the double mutant is severely impaired (Fig. S5). However, the V_{max} for Mn^{2+} reduced more than the V_{max} for Ca^{2+}, resulting in a remarkably high $V_{max(Ca)}/V_{max(Mn)}$ ratio (Fig. 7*D*). Furthermore, the back-inhibition of the double mutant already takes place at lower Ca^{2+} or Mn^{2+} concentrations than WT (Fig. S2, *C* and *D*). Thus, disrupting the N-terminal motif by two alanine mutations dramatically impairs the overall activity of SPCA1a. However, the difference between the ATPase and EP results of the double mutant suggests a more complex regulatory mechanism that most likely also involves downstream steps in EP turnover. In conclusion, Ca^{2+} binding at the EF-hand–like motif in the N terminus of SPCA1a is at least partially responsible for the biphasic stimulation pattern of SPCA1a autophosphorylation, and contributes to the lower Ca^{2+} affinity and higher maximal activity of SPCA1a *versus* SPCA2.

Discussion

In the present study, we compared the properties of the Golgi/secretory pathway Ca^{2+}/Mn^{2+}-ATPases SPCA1a and SPCA2 in a purified, reconstituted system. We report isoform-specific differences between the Ca^{2+}- and Mn^{2+}-dependent properties of SPCA1a and SPCA2 that can at least in part be attributed to a Ca^{2+}-binding regulatory motif in the N terminus of SPCA1a, which is absent in SPCA2.

An N-terminal EF-hand–like motif regulates the ion affinity and maximal activity of SPCA1a

Via a diverse set of approaches on purified SPCA1a and N-terminal fragments, we revealed a previously unrecognized Ca^{2+}-dependent regulatory element that is present in SPCA1a, but absent in SPCA2. First, we observed a biphasic curve for SPCA1a autophosphorylation, which points to a regulatory mechanism that controls the activation state in a substrate-dependent manner. Second, we found that Ca^{2+} stimulates SPCA1a's EP formation more than Mn^{2+}, in line with a Ca^{2+}-specific regulatory site. Third, through NMR experiments, we confined the Ca^{2+} binding to specific Ca^{2+}-coordinating residues belonging to the EF-hand–like motif in the SPCA1a N terminus. No Mn^{2+} binding was observed to this site. Fourth, Ca^{2+} alters the mobility of purified SPCA1a on native PAGE, which is less clear with Mn^{2+} or with mutations in the EF-hand–like motif. Fifth, via mutagenesis we demonstrated that the EF-hand–like motif contributes to the stronger Ca^{2+}-dependent activation of autophosphorylation, the higher turnover rate and lower apparent Ca^{2+} affinity of SPCA1a as compared with SPCA2. In contrast, the mutations minimally affect the Mn^{2+} properties of SPCA1a. Taken together, the N-terminal EF-hand–like motif specifically binds Ca^{2+} and contributes to the isoform-specific properties of SPCA1a.

Besides the EF-hand–like motif, also the ATP concentration critically influences (i) the apparent Ca^{2+} affinity, and (ii) biphasic activation behavior of SPCA1a. Indeed, we first observed that the Ca^{2+} affinity of SPCA1a in the autophosphorylation assay at 5 μM ATP is unusually low, whereas SPCA1a's Ca^{2+} affinity increases at higher ATP concentrations. Conversely, reducing the ATP concentration in the ATPase assay lowers the apparent Ca^{2+} affinity of SPCA1a. Second, the biphasic activation pattern of SPCA1a is most clear at low ATP concentrations in both the autophosphorylation (Fig. 2*E*) and ATPase assay (Fig. S3). Moreover, the ATP concentration determines the Ca^{2+} sensitivity of the SPCA1a activation. At 0.5 mM ATP, the second activation step takes place between 1 and 10 μM Ca^{2+} (Fig. S3), *i.e.* at physiological Ca^{2+} concentrations. However, at 5 μM ATP, Ca^{2+} concentrations between 30 μM and 3 mM are required to trigger maximal autophosphorylation, *i.e.* well above physiological Ca^{2+} concentrations.

We therefore conclude that at high Ca^{2+} concentrations, Ca^{2+} binds to the N-terminal EF-hand–like motif of SPCA1a, and activates it. In contrast, at low Ca^{2+} concentrations SPCA1a is in a less active state due to the lack of Ca^{2+} binding to the EF-hand–like motif, which hinders autophosphorylation. Overall, this explains the low apparent Ca^{2+} affinity of SPCA1a and its higher Ca^{2+}-dependent ATPase activity. We showed that this system is sensitive to the ATP concentration. When the ATP concentration is low, a Ca^{2+} concentration above 10 μM is required to maximally activate SPCA1a, whereas at more physiological ATP concentrations a Ca^{2+} level between 1 and 10 μM is sufficient to maximally activate SPCA1a. These observations suggest that ATP binding and N-terminal regulation are mechanistically linked.

It is not entirely clear how the N terminus may regulate the relative substrate affinities or how ATP may control this system. Because the distal N-terminal region is not directly involved in Ca^{2+} coordination in the membrane domain, it most likely modulates the substrate affinity indirectly. The N terminus may influence the packing of the Ca^{2+}- and or Mn^{2+}-coordinating residues in the ion entry/exit channels in the membrane domain or at the substrate-binding site. The ionic

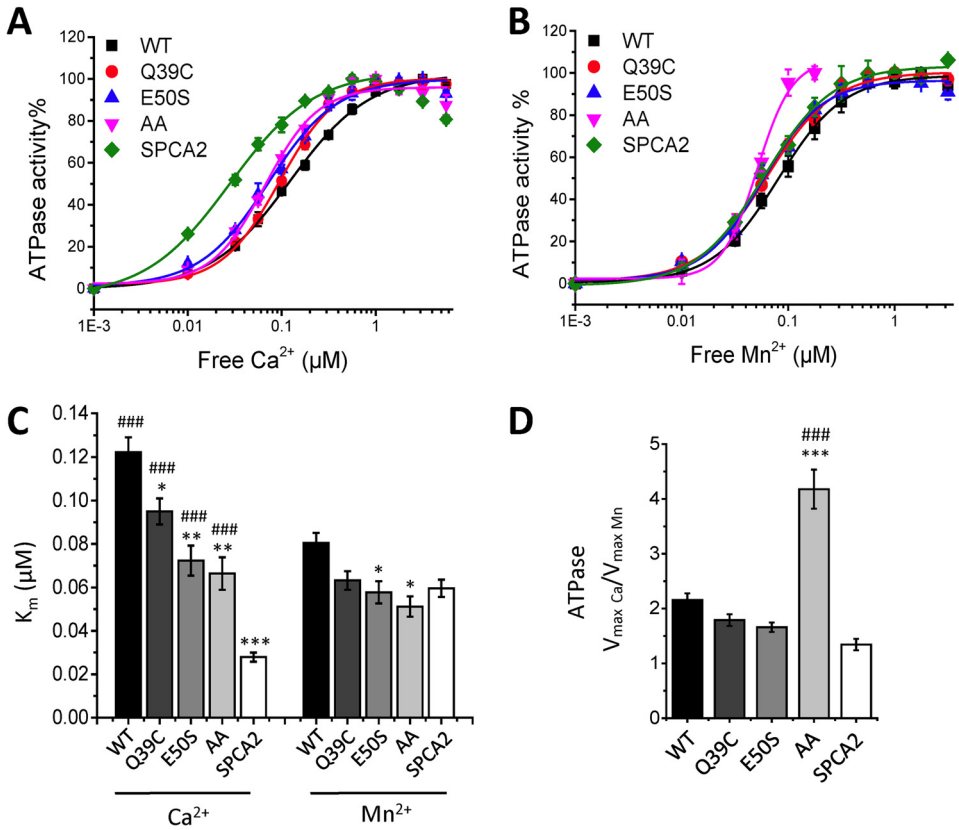

Figure 7. ATPase activities of SPCA1a WT and N-terminal EF-hand–like mutants. *A* and *B*, Ca^{2+}- and Mn^{2+}-dependent ATPase activities were measured on all constructs and fitted with logistic curves. Bar graphs depict the apparent ion affinities (K_m, *C*) and the ratio of maximal ATPase activities with Ca^{2+} over Mn^{2+} (*D*) ($n = 3$). Statistical analysis was performed using one-way ANOVA followed by a post hoc Bonferroni test. *, significantly different from SPCA1a WT. #, significantly different from SPCA2. *, $p < 0.05$; **, $p < 0.01$; ***, $p < 0.001$.

radius of Mn^{2+} (0.8 Å) is smaller than that of Ca^{2+} (0.99 Å) (36) and the N terminus may induce a local change at the ion-binding sites that differently affects the ion affinity. Alternatively, the N terminus of SPCA1a may modulate the conformational transitions in the catalytic cycle. A reduced apparent Ca^{2+} affinity may, for instance, be explained by stabilizing the SPCA1a protein more in the E2 than E1 state.

Both models depend on the interaction of the N terminus with downstream elements of the pump. Such a mode of action was already proposed for the yeast PMR1 protein. PMR1 also contains a Ca^{2+} binding N-terminal EF-hand–like motif that regulates the substrate affinities and Ca^{2+}/Mn^{2+} selectivity, and a partial proteolytic digestion analysis indicated that the N-terminal region may interact with the catalytic ATP-binding domain of PMR1 (21). An interaction between the N terminus and the ATP-binding domain may offer a mechanistic explanation of how ATP may modulate the regulation by the N terminus. Future work will focus on identifying the interacting site of the N terminus in SPCA1a, which will further reveal the mechanism of SPCA1a activation.

Post-translational modifications may influence SPCA1a activity in a cellular context

In a previous report from our lab we compared the biochemical properties of SPCA1d and SPCA2 in membrane fractions of HEK-293 overexpressing cells (27). In that study, SPCA1d and SPCA2 displayed a similar apparent affinity in the ATPase assay (K_m of 0.041 and 0.037 μM, respectively), whereas the catalytic turnover rate of SPCA1a was lower (27). This is clearly different from the measurements on purified SPCA1a and SPCA2 in this study. Also the biphasic activation pattern of SPCA1a was not observed before. Because the SPCA1a and SPCA1d splice variants only differ in the C terminus and contain the same N terminus, the discrepancies between both studies may not merely reflect differences between splice variants. Instead, several factors may influence the N-terminal activation mechanism in a cellular context, such as post-translational modifications, lipid interactions, or regulatory proteins that are absent in the purified systems. In that respect, we observed remarkable differences in the mobility of SPCA1a in HEK-293 microsomes *versus* proteoliposomes. The purified SPCA1a from yeast runs as a single monomer and single dimer band (Fig. 1*A*), whereas we, and others (14, 37, 38), observe that monomers of the SPCA1 splice variants in mammalian membrane fractions migrate as a double band (Fig. S6*A*). Remarkably, the lower band of SPCA1a in microsomes diminishes after treatment with reducing agent in combination with heating, and the higher band becomes stronger, which is not observed for SPCA1a in proteoliposomes (Fig. S6*B*). This may point to post-translational modifications of SPCA1a, such as disulfide bridges, which are only present in microsomes. These modifications may influence the biochemical properties, possibly explaining the difference between SPCA1a in proteoliposomes and in microsomes. These intrigu-

ing observations may point to an unknown regulatory system of SPCA1a in the cell, but future studies are needed to clarify this point. Analyzing the purified proteins, *i.e.* in the absence of confounding cellular elements, revealed an N-terminal regulatory element in SPCA1a, which otherwise would have been missed in the microsome context.

Physiological implications of the Ca^{2+}-dependent regulation of SPCA1a

We compared the biochemical properties of purified SPCA1a and SPCA2 proteins in a fixed membrane environment, which eliminated cell-based confounding factors. The two human SPCA isoforms present different affinities and turnover rates toward Ca^{2+} and Mn^{2+} ions, their preferred substrates. SPCA1a displayed a 2-fold higher maximal turnover rate with Ca^{2+} than with Mn^{2+}, whereas SPCA2 presented similar turnover rates for both substrates. In addition, the two isoforms exhibited similar Mn^{2+} affinities, whereas the apparent Ca^{2+} affinity of SPCA1a is significantly lower as compared with SPCA2.

These isoform-specific properties may have important physiological implications. Due to its extremely high Ca^{2+} affinity, but 2-fold lower Mn^{2+} affinity, SPCA2 may mainly transport Ca^{2+} ions. The dominant Ca^{2+} transport function of SPCA2 may be relevant for secretory cells where SPCA2 is predominantly expressed (7, 8). In secretory cell types like mammary gland, SPCA2 is functionally coupled to the Orai1 Ca^{2+} channel where it transports Ca^{2+} that comes in from the extracellular environment via Orai1 into the secretory pathway (11, 13). In contrast, SPCA1a is ubiquitously expressed and fulfills a housekeeping function by delivering both Ca^{2+} and Mn^{2+} into the Golgi/secretory compartment to support protein folding and maturation (3). The slightly higher affinity of SPCA1a for Mn^{2+} than Ca^{2+} suggests that at low ion availability the relative Ca^{2+} and Mn^{2+} concentrations will determine which ion will be transported by SPCA1a.

Our biochemical analysis further suggests that depending on the Ca^{2+} and ATP concentration, the EF-hand–like motif may switch SPCA1a between a high affinity/low capacity Ca^{2+}/Mn^{2+} pump to a lower affinity, but higher capacity Ca^{2+} pump. Consequently, SPCA1a presents a higher Ca^{2+} transport capacity when the cytosolic Ca^{2+} load increases, which may occur in cell types undergoing Ca^{2+} signaling or fulfilling secretory functions. Like SPCA2, SPCA1a expression is elevated in mammary gland during lactation (14, 38), and both isoforms may operate together to transfer Ca^{2+} into the milk (11, 13). Although SPCA2 may be the major activator of Orai1 (11), SPCA1a may present a higher Ca^{2+} transport capacity than SPCA2. SPCA1a is detected in the subplasma membrane region close to the plasma membrane Ca^{2+} channel Orai1, where it may participate in SICE (13) and may become fully activated by the local Ca^{2+} increase (up to 300 μM in microdomains near Ca^{2+} channels (39)). Our data suggest that SPCA2 may not be further activated by Ca^{2+}, but this does not exclude that the SPCA2 activity may respond to other stimuli such as the direct interaction with Orai1.

Mutations in SPCA1a lead to the skin disease Hailey–Hailey, which is manifested in the keratinocytes. Keratinocytes undergo substantial changes in their intracellular ATP and Ca^{2+} concentrations, and in this context, SPCA1a regulation by the EF-hand–like motif may take place. Keratinocytes contain merely one-third to one-fourth of the ATP concentration of artery smooth muscle cells (40). These low ATP levels further decrease when extracellular Ca^{2+} levels are increased (40), which may resemble the situation in the outer layers of the skin epidermis where extracellular Ca^{2+} progressively increases (41). The local environment with low ATP and high Ca^{2+} concentrations may affect the activity of SPCA1 via the N-terminal EF-hand–like motif. Moreover, in isolated keratinocytes of Hailey–Hailey disease patients with dysfunctional SPCA1, the ATP concentration is reduced, whereas the ATP levels fail to increase when extracellular Ca^{2+} is supplied (40). The altered ATP and Ca^{2+} concentrations in Hailey–Hailey disease may contribute to the dysregulation of SPCA1a activity.

In conclusion, our work on purified SPCA1a and SPCA2 proteins provides a comprehensive analysis of the isoform-specific Ca^{2+}- and Mn^{2+}-dependent activities. We discovered a Ca^{2+}-binding EF-hand–like motif in the N terminus of SPCA1a that is absent in SPCA2. This motif is at least partially responsible for the SPCA1a-specific biochemical properties. Depending on the ATP concentration, the N terminus switches SPCA1a between a high affinity/low capacity state at low Ca^{2+} concentrations, and a low affinity/high capacity state at high Ca^{2+} loads. This mechanism may play a role in secreting cells like mammary gland during lactation, or in keratinocytes in the outer layers of the skin epidermis.

Experimental procedures

Plasmids and mutagenesis

The C-terminal His_8-tagged human SPCA1a WT or mutants were introduced via Q5 site-directed mutagenesis (New England Biolabs) as previously described (23). The C-terminal His_{10}-tagged human SPCA2 in the pADANS vector was a kind gift from Dr. S. Yamamoto, Kyorin University School of Medicine (42).

Purification and reconstitution of SPCA1a/2

Vectors containing SPCA1a and SPCA2 WT or mutants were transformed into *S. cerevisiae* strain BY4741a (his3Δ1; leu2Δ0;met15Δ0;ura3Δ0;MATa) as previously described (23). Each yeast clone was inoculated in minimal medium deprived of Leu for selection, then grown in yeast peptone dextrose medium for 30 h before harvesting. Yeast cells were pelleted at 5,000 × *g* for 5 min, 4 °C, washed with Milli-Q water, flash-frozen, and stored at −20 °C. The membrane fractions of yeast were isolated via differential centrifugations as previously described (23). The purification of His-tagged SPCA1a and SPCA2 proteins was performed by nickel-nitrilotriacetic acid affinity chromatography (23). Reconstitution of SPCA1a and SPCA2 in proteolipsomes composed of 80% phosphatidylcholine and 20% phosphatidic acid (Avanti Polar Lipids) was performed following the protocol in Ref. 23.

SDS protein electrophoresis and protein quantification

Purified or reconstituted SPCA1a or SPCA2 was separated on a NuPAGE 4–12% BisTris polyacrylamide gel (200 V, 35

min, MES buffer) (Thermo Fisher Scientific) and visualized with Imperial Protein Stain (Thermo Fisher Scientific). SeeBlue Plus2 Pre-stained Protein Standard (Thermo Fisher Scientific) was used as a molecular weight marker. The concentration of purified protein was determined by direct comparison to a bovine serum albumin (BSA) standard on the same gel (BSA Standard Ampules, Pierce).

Native PAGE

Purified proteins were incubated for 15 min at room temperature in buffer containing 100 mM MOPS, pH 7.0, 1 mM EGTA, 160 mM KCl, 0.2 mg/ml of dodecyl maltoside and $CaCl_2$ or $MnCl_2$ to reach the final Ca^{2+} or Mn^{2+} concentration indicated in the experimental conditions. The samples were then mixed with 4× native PAGE sample buffer supplemented with NativePAGE™ 5% G-250 Sample Additive according to the instructions from the manufacturer. The electrophoresis was performed at 150 V for 100 min at room temperature using native PAGE running buffer as the anode buffer, and the cathode buffer was supplemented with 0.02% Coomassie Blue G-250. The native PAGE gel, sample buffer, sample additive and Coomassie Blue G-250 were purchased from Thermo Fisher Scientific. The protein bands were visualized by destaining or immunoblotting.

ATPase assay

The ATPase activity of reconstituted samples was assayed by a colorimetric assay via the detection of P_i in the presence of 5 mM ATP, as previously described (43). The reactions were performed for 30 min using 300 ng of purified SPCA1a or SPCA2 in a reaction volume of 50 μl. The ATPase measurements with lower ATP concentrations were performed using the NADH-coupled assay in a 96-well plate. A total reaction mix of 250 μl contained 100 ng of purified SPCA1a, 50 mM TES/Tris, pH 7, 100 mM KCl, 7 mM $MgCl_2$, 1 mM EGTA, 0.36 mM NADH, 1 mM phosphoenolpyruvate, 2.4 units of pyruvate kinase, 2.4 units of lactate dehydrogenase and the indicated free Ca^{2+} concentrations. The reaction was started by addition of the required amount of ATP. After 20 s mixing, the absorbance was read at 340 nm over 10 min in 30-s intervals with a SPECTRAmax PLUS^{384} Microplate Spectrophotometer (Molecular Devices). The slope of the decreased absorbance over time was used as a measure of the ATPase rate. All products were purchased from Merck.

Autophosphorylation assay

The autophosphorylation reaction was performed as described in Ref. 44 with slight modifications. Briefly, the reaction mixture contains 0.5 μg of purified SPCA1a or SPCA2 and 40 μg of BSA in a buffer containing 160 mM KCl, 17 mM Hepes, pH 7.0, 1 mM DTT, 5 mM $MgCl_2$, 1 mM EGTA and various concentration of $CaCl_2$, $MnCl_2$, or $MgCl_2$ as indicated in the experimental conditions. Unless specified otherwise, all autophosphorylation experiments were performed with 5 mM Mg^{2+}. The reaction was initiated by addition of 0.074 MBq of radioactively labeled [γ-^{32}P]ATP (PerkinElmer Life Sciences) in a final concentration of 5 μM. After a 20-s reaction on ice, 500 μl of stop solution containing 6% TCA, 10 mM phosphoric acid, and 1 mM ATP was added to the reaction mixture for precipitation. The pellet was washed three times with stop solution before detection in a scintillation counter (Packard, 2900TR) or by running on an acidic gel as previously described (44) and then detected with a phosphorimager (Typhoon, FLA9500). For HA treatment an additional washing step with 0.25 M HA was performed.

NMR analysis

A GST-labeled N-terminal fragment of the human SPCA1a (Val-20 to Glu-67) was cloned in the pET41a(+) vector and expressed in BL21 *Escherichia coli* with ^{15}N-enriched growth medium. After affinity purification and thrombin cleavage to remove GST, a 59-amino acid long peptide (HsSPCA1-short) was obtained that consists of a 9-residue long linker (SPMGYRGSM) and the N-terminal SPCA1a sequence (^{20}VLTSKK-ASELPVSEVASILQADLQNGLNKCVSHRRAFHGWNEFDI-SEDE^{69}). NMR experiments were conducted with a Bruker Avance 600 MHz (^{1}H) Ultrashield™ Plus with a CP TCI 600 S3 H-C/N-D-05 Z probe (Bruker, Fällanden, Switzerland). All data were processed using the TopSpin software (version 3.2) provided by Bruker and the resulting spectra were analyzed using the computer-aided resonance assignment software. ^{1}H,^{15}N-HSQC spectra (45, 46) were recorded at 5 °C using 12 scans with 4096 data points in the t_2 dimension and 200 data points in the t_1 dimension. The spectral width for the t_1 dimension was 2311 Hz (38 ppm) and for the t_2 dimension 9615 Hz (16 ppm). During each titration step, 0.5 μl of a $CaCl_2$ solution (0.5 M) was added. After the Ca^{2+} titration, 5 μl of a $MnSO_4$ solution (0.1 mM) was added to verify interactions between the SPCA1 N terminus and Mn^{2+}.

Statistical analysis

Values are provided as mean ± S.E. from a n number of independent measurements. Radiograms and gel images are representative for a minimum of $n = 3$ experiments. Logistic fitting was performed via OriginPro 9 software. Statistical significance was calculated by one-way ANOVA followed by a Bonferroni post hoc test and indicated by asterisks: *, $p < 0.05$; **, $p < 0.01$; ***, $p < 0.001$.

Author contributions—J. C., F. W., and P. V. conceptualization; J. C., S. S., and C.-A. M. formal analysis; J. C. validation; J. C., S. S., C.-A. M., F. P., I. V., J. V., E. L., and P. V. investigation; J. C. visualization; J. C., C.-A. M., I. V., J. V., E. L., and P. V. methodology; J. C. and P. V. writing-original draft; J. C., J. E., and P. V. writing-review and editing; E. L. and P. V. resources; E. L., J. E., and P. V. supervision; P. V. funding acquisition; P. V. project administration.

References

1. Berridge, M. J., Bootman, M. D., and Roderick, H. L. (2003) Calcium signalling: dynamics, homeostasis and remodelling. *Nat. Rev. Mol. Cell Biol.* **4,** 517–529 CrossRef Medline
2. Monteith, G. R., McAndrew, D., Faddy, H. M., and Roberts-Thomson, S. J. (2007) Calcium and cancer: targeting Ca^{2+} transport. *Nat. Rev. Cancer* **7,** 519–530 CrossRef Medline
3. Vangheluwe, P., Sepúlveda, M. R., Missiaen, L., Raeymaekers, L., Wuytack, F., and Vanoevelen, J. (2009) Intracellular Ca^{2+}- and Mn^{2+}-transport ATPases. *Chem. Rev.* **109,** 4733–4759 CrossRef Medline

4. Sepulveda, M. R., Dresselaers, T., Vangheluwe, P., Everaerts, W., Himmelreich, U., Mata, A. M., and Wuytack, F. (2012) Evaluation of manganese uptake and toxicity in mouse brain during continuous $MnCl_2$ administration using osmotic pumps. *Contrast Media Mol. Imaging* **7,** 426–434 CrossRef Medline
5. Leitch, S., Feng, M., Muend, S., Braiterman, L. T., Hubbard, A. L., and Rao, R. (2011) Vesicular distribution of secretory pathway Ca^{2+}-ATPase isoform 1 and a role in manganese detoxification in liver-derived polarized cells. *Biometals* **24,** 159–170 CrossRef Medline
6. Hu, Z., Bonifas, J. M., Beech, J., Bench, G., Shigihara, T., Ogawa, H., Ikeda, S., Mauro, T., and Epstein, E. H., Jr. (2000) Mutations in ATP2C1, encoding a calcium pump, cause Hailey-Hailey disease. *Nat. Genet.* **24,** 61–65 CrossRef Medline
7. Xiang, M., Mohamalawari, D., and Rao, R. (2005) A novel isoform of the secretory pathway Ca^{2+}, Mn^{2+}-ATPase, hSPCA2, has unusual properties and is expressed in the brain. *J. Biol. Chem.* **280,** 11608–11614 CrossRef Medline
8. Vanoevelen, J., Dode, L., Van Baelen, K., Fairclough, R. J., Missianen, L., Raeymaekers, L., and Wuytack, F. (2005) The secretory pathway Ca^{2+}/Mn^{2+}-ATPase 2 is a Golgi-localized pump with high affinity for Ca^{2+} ions. *J. Biol. Chem.* **280,** 22800–22808 CrossRef Medline
9. Baron, S., Struyf, S., Wuytack, F., Van Damme, J., Missiaen, L., Raeymaekers, L., and Vanoevelen, J. (2009) Contribution of intracellular Ca^{2+} stores to Ca^{2+} signaling during chemokinesis of human neutrophil granulocytes. *Biochim. Biophys. Acta* **1793,** 1041–1049 CrossRef Medline
10. Faddy, H. M., Smart, C. E., Xu, R., Lee, G. Y., Kenny, P. A., Feng, M., Rao, R., Brown, M. A., Bissell, M. J., Roberts-Thomson, S. J., and Monteith, G. R. (2008) Localization of plasma membrane and secretory calcium pumps in the mammary gland. *Biochem. Biophys. Res. Commun.* **369,** 977–981 CrossRef Medline
11. Feng, M., Grice, D. M., Faddy, H. M., Nguyen, N., Leitch, S., Wang, Y., Muend, S., Kenny, P. A., Sukumar, S., Roberts-Thomson, J. J., Monteith, G. R., and Rao, R. (2010) Store-independent activation of Orai1 by SPCA2 in mammary tumors. *Cell* **143,** 84–98 Medline
12. Smaardijk, S., Chen, J., Wuytack, F., and Vangheluwe, P. (2017) SPCA2 couples Ca^{2+} influx via Orai1 to Ca^{2+} uptake into the Golgi/secretory pathway. *Tissue Cell* **49**, 141–149 CrossRef Medline
13. Smaardijk, S., Chen, J., Kerselaers, S., Voets, T., Eggermont, J., and Vangheluwe, P. (2018) Store-independent coupling between the secretory pathway Ca^{2+} transport ATPase SPCA1 and Orai1 in Golgi stress and Hailey-Hailey disease. *Biochim. Biophys. Acta* **1865,** 855–862 CrossRef
14. Cross, B. M., Hack, A., Reinhardt, T. A., and Rao, R. (2013) SPCA2 regulates Orai1 trafficking and store independent Ca^{2+} entry in a model of lactation. *PLoS ONE* **8,** e67348 CrossRef Medline
15. Cross, B. M., Breitwieser, G. E., Reinhardt, T. A., and Rao, R. (2014) Cellular calcium dynamics in lactation and breast cancer: from physiology to pathology. *Am. J. Physiol. Cell Physiol.* **306,** C515–C526 CrossRef
16. Dang, D., Prasad, H., and Rao, R. (2017) Secretory pathway Ca^{2+}-ATPases promote *in vitro* microcalcifications in breast cancer cells. *Mol. Carcinogen.* **56,** 2474–2485 CrossRef
17. Grice, D. M., Vetter, I., Faddy, H. M., Kenny, P. A., Roberts-Thomson, S. J., and Monteith, G. R. (2010) Golgi calcium pump secretory pathway calcium ATPase 1 (SPCA1) is a key regulator of insulin-like growth factor receptor (IGF1R) processing in the basal-like breast cancer cell line MDA-MB-231. *J. Biol. Chem.* **285,** 37458–37466 CrossRef Medline
18. Sitsel, A., De Raeymaecker, J., Drachmann, N. D., Derua, R., Smaardijk, S., Andersen, J. L., Vandecaetsbeek, I., Chen, J., De Maeyer, M., Waelkens, E., Olesen, C., Vangheluwe, P., and Nissen, P. (2019) Structures of the heart specific SERCA2a Ca^{2+}-ATPase. *EMBO J.* **38,** e100020 CrossRef Medline
19. Gong, D., Chi, X., Ren, K., Huang, G., Zhou, G., Yan, N., Lei, J., and Zhou, Q. (2018) Structure of the human plasma membrane Ca^{2+}-ATPase 1 in complex with its obligatory subunit neuroplastin. *Nat. Commun.* **9,** 3623 CrossRef Medline
20. Lopreiato, R., Giacomello, M., and Carafoli, E. (2014) The plasma membrane calcium pump: new ways to look at an old enzyme. *J. Biol. Chem.* **289,** 10261–10268 CrossRef Medline
21. Wei, Y., Marchi, V., Wang, R., and Rao, R. (1999) An N-terminal EF hand-like motif modulates ion transport by Pmr1, the yeast Golgi Ca^{2+}/Mn^{2+}-ATPase. *Biochemistry* **38,** 14534–14541 CrossRef Medline
22. Mandal, D., Woolf, T. B., and Rao, R. (2000) Manganese selectivity of pmr1, the yeast secretory pathway ion pump, is defined by residue Gln-783 in transmembrane segment 6: residue Asp-778 is essential for cation transport. *J. Biol. Chem.* **275,** 23933–23938 CrossRef Medline
23. Chen, J., De Raeymaecker, J., Hovgaard, J. B., Sammrdijk, S., Vandecaetsbeek, I., Wuytack, F., Møller, J. V., Eggermont, J., De Maeyer, M., Christensen, S. B., and Vangheluwe, P. (2017) Structure/activity relationship of thapsigargin inhibition on the purified Golgi/secretory pathway Ca^{2+}/Mn^{2+}-transport ATPase (SPCA1a). *J. Biol. Chem.* **292,** 6938–6951 CrossRef Medline
24. Baginski, E. S., Foà, P. P., and Zak, B. (1967) Microdetermination of inorganic phosphate, phospholipids, and total phosphate in biologic materials. *Clin. Chem.* **13,** 326–332 Medline
25. Kühlbrandt, W. (2004) Biology, structure and mechanism of P-type ATPases. *Nat. Rev. Mol. Cell Biol.* **5,** 282–295 CrossRef Medline
26. Ton, V. K., Mandal, D., Vahadji, C., and Rao, R. (2002) Functional expression in yeast of the human secretory pathway Ca^{2+}, Mn^{2+}-ATPase defective in Hailey-Hailey disease. *J. Biol. Chem.* **277,** 6422–6427 CrossRef Medline
27. Dode, L., Andersen, J. P., Vanoevelen, J., Raeymaekers, L., Missiaen, L., Vilsen, B., and Wuytack, F. (2006) Dissection of the functional differences between human secretory pathway Ca^{2+}/Mn^{2+}-ATPase (SPCA) 1 and 2 isoenzymes by steady-state and transient kinetic analyses. *J. Biol. Chem.* **281,** 3182–3189 CrossRef Medline
28. Dode, L., Andersen, J. P., Raeymaekers, L., Missiaen, L., Vilsen, B., and Wuytack, F. (2005) Functional comparison between secretory pathway Ca^{2+}/Mn^{2+}-ATPase (SPCA) 1 and sarcoplasmic reticulum Ca^{2+}-ATPase (SERCA) 1 isoforms by steady-state and transient kinetic analyses. *J. Biol. Chem.* **280,** 39124–39134 CrossRef Medline
29. Lytton, J., Westlin, M., Burk, S. E., Shull, G. E., and MacLennan, D. H. (1992) Functional comparisons between isoforms of the sarcoplasmic or endoplasmic reticulum family of calcium pumps. *J. Biol. Chem.* **267,** 14483–14489 Medline
30. Post, R. L., and Kume, S. (1973) Evidence for an aspartyl phosphate residue at the active site of sodium and potassium ion transport adenosine triphosphatase. *J. Biol. Chem.* **248,** 6993–7000 Medline
31. Bolton, E. C., Mildvan, A. S., and Boeke, J. D. (2002) Inhibition of reverse transcription *in vivo* by elevated manganese ion concentration. *Mol. Cell* **9,** 879–889 CrossRef Medline
32. Beckman, R. A., Mildvan, A. S., and Loeb, L. A. (1985) On the fidelity of DNA replication: manganese mutagenesis *in vitro*. *Biochemistry* **24,** 5810–5817 CrossRef Medline
33. Drmota Prebil, S. D., Slapšak, U., Pavšič, M., Ilc, G., Puž, V., de Almeida Ribeiro, E., Anrather, D., Hartl, M., Backman, L., Plavec, J., Lenarčič, B., and Djinović-Carugo, K. (2016) Structure and calcium-binding studies of calmodulin-like domain of human non-muscle α-actinin-1. *Sci. Rep.* **6,** 27383 CrossRef Medline
34. Rule, G. S., and Hitchens, T. K. (2006) Fundamentals of protein NMR spectroscopy. in *Focus on Structural Biology* (Kaptein, R., ed) pp. 530, Springer, Dordrecht
35. Zhou, Y., Frey, T. K., and Yang, J. J. (2009) Viral calciomics: interplays between Ca^{2+} and virus. *Cell Calcium* **46,** 1–17 CrossRef Medline
36. Moody, B. J. (1991) *Comparative Inorganic Chemistry* (Bernard, M., ed) 3rd Ed, pp. xiii and 562, Academic Press, Washington, D. C
37. Sepúlveda, M. R., Marcos, D., Berrocal, M., Raeymaekers, L., Mata, A. M., and Wuytack, F. (2008) Activity and localization of the secretory pathway Ca^{2+}-ATPase isoform 1 (SPCA1) in different areas of the mouse brain during postnatal development. *Mol. Cell. Neurosci.* **38,** 461–473 CrossRef Medline
38. Reinhardt, T. A., Filoteo, A. G., Penniston, J. T., and Horst, R. L. (2000) Ca^{2+}-ATPase protein expression in mammary tissue. *Am. J. Physiol. Cell Physiol* **279,** C1595–1602 CrossRef Medline
39. Llinás, R., Sugimori, M., and Silver, R. B. (1992) Microdomains of high calcium concentration in a presynaptic terminal. *Science* **256,** 677–679 CrossRef Medline

40. Aronchik, I., Behne, M. J., Leypoldt, L., Crumrine, D., Epstein, E., Ikeda, S., Mizoguchi, M., Bench, G., Pozzan, T., and Mauro, T. (2003) Actin reorganization is abnormal and cellular ATP is decreased in Hailey-Hailey keratinocytes. *J. Investig. Dermatol.* **121,** 681–687 CrossRef Medline
41. Elias, P., Ahn, S., Brown, B., Crumrine, D., and Feingold, K. R. (2002) Origin of the epidermal calcium gradient: regulation by barrier status and role of active *vs* passive mechanisms. *J. Investig. Dermatol.* **119,** 1269–1274 CrossRef Medline
42. Yamamoto, S., Takehara, M., Kabashima, Y., Fukutomi, T., and Ushimaru, M. (2016) Identification of novel inhibitors of human SPCA2. *Biochem. Biophys. Res. Commun.* **477,** 266–270 CrossRef Medline
43. Vandecaetsbeek, I., Holemans, T, Wuytack, F., and Vangheluwe, P. (2014) High-throughput measurement of the Ca^{2+}-dependent ATPase activity in COS microsomes. *Cold Spring Harb. Protoc.* **2014,** 865–875 Medline
44. Holemans, T., Sørensen, D. M., van Veen, S., Martin, S., Hermans, D., Kemmer, G. C., Van den Haute, C., Baekelandt, V., Günther Pomorski, T., Agostinis, P., Wuytack, F., Palmgren, M., Eggermont, J., and Vangheluwe, P. (2015) A lipid switch unlocks Parkinson's disease-associated ATP13A2. *Proc. Natl. Acad. Sci. U.S.A.* **112,** 9040–9045 CrossRef Medline
45. Davis, A. L., Keeler, J., Laue, E. D., and Moskau, D. (1992) Experiments for recording pure-absorption heteronuclear correlation spectra using pulsed field gradients. *J. Magn. Res.* **98,** 207–216 CrossRef
46. Grzesiek, S., and Bax, A. (1993) The importance of not saturating H_2O in protein NMR: application to sensitivity enhancement and NOE measurements. *J. Am. Chem. Soc.* **115,** 12593–12594 CrossRef